AIP | Applied Physics Letters

Efficient needle plasma actuators for flow control and surface cooling

Pengfei Zhao, Sherlie Portugal, and Subrata Roy

Citation: Applied Physics Letters **107**, 033501 (2015); doi: 10.1063/1.4927051
View online: http://dx.doi.org/10.1063/1.4927051
View Table of Contents: http://scitation.aip.org/content/aip/journal/apl/107/3?ver=pdfcov
Published by the AIP Publishing

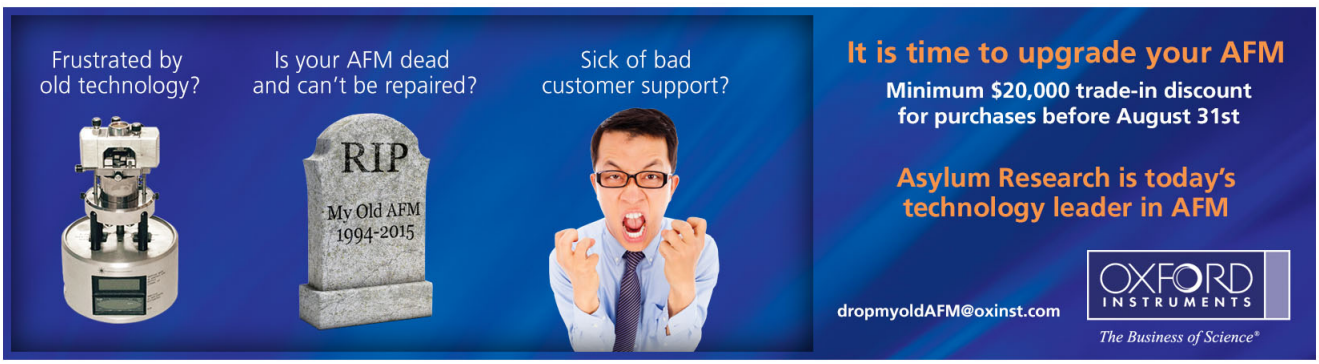

Efficient needle plasma actuators for flow control and surface cooling

Pengfei Zhao, Sherlie Portugal, and Subrata Roy[a)]
Applied Physics Research Group, Department of Mechanical and Aerospace Engineering, University of Florida, Gainesville, Florida 32611, USA

(Received 30 April 2015; accepted 8 July 2015; published online 20 July 2015)

We introduce a milliwatt class needle actuator suitable for plasma channels, vortex generation, and surface cooling. Electrode configurations tested for a channel configuration show 1400% and 300% increase in energy conversion efficiency as compared to conventional surface and channel corona actuators, respectively, generating up to 3.4 m/s air jet across the channel outlet. The positive polarity of the needle is shown to have a beneficial effect on actuator efficiency. Needle-plate configuration is demonstrated for improving cooling of a flat surface with a 57% increase in convective heat transfer coefficient. Vortex generation by selective input signal manipulation is also demonstrated. © *2015 AIP Publishing LLC*. [http://dx.doi.org/10.1063/1.4927051]

Atmospheric plasma driven active flow control devices have been extensively studied in recent years.[1–5] Applications of these devices range from control of the laminar to turbulent transition,[6] drag reduction,[7] to surface cooling.[8] The most common example is the dielectric barrier discharge (DBD) actuator. Advantages of DBD actuator include lack of moving parts, fast response, small scale, surface compliance, and ease of construction and application. However, major disadvantage of such device is that their energy conversion efficiencies are extremely low (∼0.1%).[2,9] This is due to a large energy loss in heating the plasma.[10] As compared to DBD, direct current (DC) corona discharge only generates minimal glow near the surface of a powered electrode. Thus, the energy loss mentioned above can be reduced. However, the energy conversion efficiencies of DC corona devices remain less than 1%.[2,3] This is due to a combination of weak plasma generation near the wire and an excessive viscous loss from the thin wall shear layer. In contrast, the channel configuration[11] with sharp needle electrode might be employed to enhance the ion generation near the needle tip and minimize the viscous loss from flow induced by plasma body force.

Typically, atmospheric DC corona discharge devices consist of a powered electrode and a grounding electrode separated by air. The powered electrode usually has a sharp tip or edge with a minute radius of curvature. The grounding electrode often has a large smooth surface. Application of a high-voltage DC signal to the powered electrode forms a surface corona discharge around the sharp tip or the round edge where the maximum electric field is generated. The grounding electrodes are placed some distance away to generate the desired electric field to induce the ions formed. Then, collisional momentum transfer between ions and neutral particles occurs in the space between the electrodes. Both positive and negative DC voltages can be used to induce flow with slightly different mechanisms.[2] For the positive corona, the ionization region is generated by anode electron avalanches near the electrode. Then, the Coulomb force repels positive ions toward the cathode. In the case of a negative corona, negative ions are created by the electron attachment and then repelled toward the anode.

This letter experimentally explores a class of DC corona needle actuators developed to generate moderate directed airflow with extremely low power consumption, thus improving the energy conversion efficiency by an order of magnitude higher than its DBD counterpart. Particular electrode arrangements for these devices demonstrated benefits for cooling enhancement and vortex generation. Specifically, the latter is a useful tool to reduce the drag and to stabilize the flow provided the pressure drag related to the needle electrode configuration is acceptable.

Two configurations were built and tested. The first one induces a channel flow as shown in Fig. 1(a). Here, a steel needle powered with high voltage is placed upstream between two plate electrodes to induce a jet at the core of the channel cross-section. With this configuration, direct momentum transfer into bulk flow occurs near the center of the channel height, consequently the flow induced should be affected by significantly less wall shear in comparison to the wall jet configuration where both electrodes are at the wall. The second configuration is shown in Fig. 1(b). In this configuration, a high-voltage-powered steel needle is placed in the upstream side of a single plate electrode. Such an arrangement should allow airflow driven by the corona discharge from the needle tip to the plate with either positive or negative DC signals. This configuration was first used to explore convective cooling effects. Also, since this configuration will generate 3D flow structures, a particular arrangement of multiple needles was then employed to generate three-dimensional vortical structures.

Detailed descriptions of dimensions and experiment setup are shown in Fig. 1 and described below. Powered needles and plate electrodes are separated by gap g in x-direction and height h in z-direction. The width of plate electrode denotes as w in the configuration. In all test cases, y-direction (span-wise) length of plate electrodes is set to be 10 cm. For channel configuration, only one needle is mounted in the configuration, while multiple needles evenly separated in y-direction (span-wise) are employed in the cooling and vortex generation setup. The needles are powered with a high voltage DC supply

[a)]Electronic mail: roy@ufl.edu. URL: http://aprg.mae.ufl.edu/roy/.

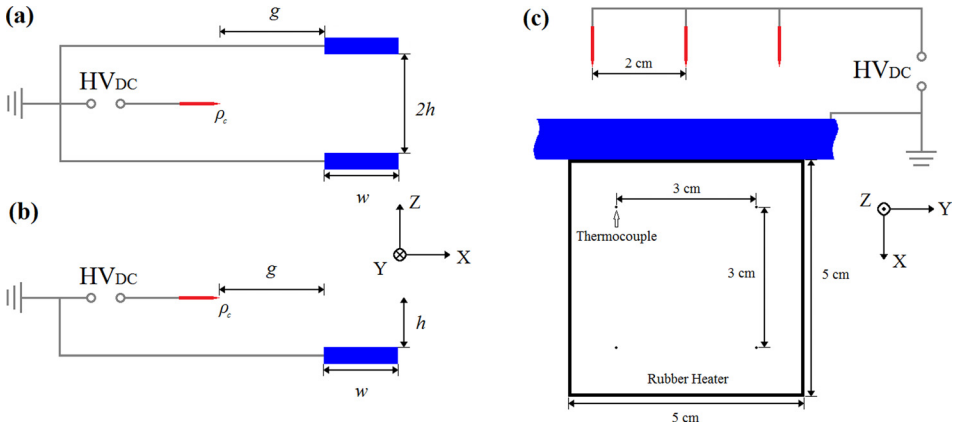

FIG. 1. Needle actuator setup: (a) Channel jet configuration, (b) single plate configuration, and (c) wall cooling jet configuration.

(TREK Model 30/20A High-Voltage Power Amplifier) and the plate electrodes are grounded. The DC signal used here is continuous with constant amplitude. All needles used in this letter have a nominal radius of curvature $\rho_c = 50\,\mu$m, and all plate electrodes are 60 μm thick and 5mm wide ($w = 5$ mm). Also, in all cases, $h = 2.5$ mm.

Electrical parameters were measured using an oscilloscope (Tektronix DPO2014) and a digital multi-meter (BK Precision 5491A). The oscilloscope has a maximum sampling rate of 1 GS/s at a bandwidth of 100 MHz. DC voltage was measured using a passive probe (Tektronix Model P6015A) with an attenuation of 1000× through the oscilloscope. The digital multi-meter of 1 mV resolution was used to measure the potential difference across a 1 MΩ resistor connected in series with the actuator. This potential difference can be converted to current with an equivalent resolution of 1 nA. Voltage and current were obtained from the measurement to calculate average electrical power using V-I method, $P_{elec} = VI$, where V and I are the average voltage and current over a 10 s period, respectively.

A LaVision particle image velocimetry (PIV) system was used to collect the velocity profile induced by channel actuators. The laser sheet used to illuminate Ondina oil seeding particles was created by a 532 nm Nd:YAG (New Wave Research Model Solo PIV II 30) laser generator fitted with a divergent cylindrical lens. Images of illuminated seeding particles were captured by a Phantom 7.3 high speed camera which has a resolution of 800 × 600 pixels on a 60 mm × 45 mm window size. LaVision's Davis 7.2 software was used to control both laser generator and high speed camera by generating external trigger through model PTU-9, programmable timing unit (synchronization resolution of 10 ns with <1 ns jitter). In this study, PIV system was employed to capture XY-plane and XZ-plane velocity profile for 3-D velocity visualization of the channel actuators and YZ-plane velocity profile to show vortex generation. According to a recent study,[12] statistical convergence for the plasma jet is within 300 samples (image pairs for correlation). Nonetheless, we took 1000 samples to eliminate the deviation.

According to the velocity profile generated from the PIV system, electro-mechanical energy conversion efficiency was obtained to evaluate the performance of the needle actuators. The induced mechanical power[2] of the airflow inside a duct is given by $P_{mec} = \frac{\rho}{2}\iint u^3 dA$, where ρ is the air density, u is the velocity at X-direction, and the 2-D integration covers all the channel cross section area A in YZ-plane. Under its definition, electro-mechanical energy conversion efficiency can be calculated as the ratio of the induced mechanical power of the airflow to the electrical power consumed in the circuit, $\eta = P_{mec}/P_{elec}$.

As previously mentioned, we used multiple needle-plate electrodes configurations to investigate the performances for various applications. The channel configuration in Fig. 1(a) was used to characterize its capability for airflow inducement. In the channel setup, gap $g = 15$ mm and channel height $2h = 5$ mm. The PIV was employed to study the three-dimensional flow structures emanating from the exit plane of the channel. The electro-mechanical energy conversion efficiency was calculated to evaluate the channel performance. Cooling effect and vortex generation were created using plate configuration (Fig. 1(b)) with multiple needles. In the cooling experiment, three needles separated by a span-wise distance of 2 cm were placed at height $h = 2.5$ mm with stream-wise gap $g = 15$ mm. One 5 × 5 cm^2 rubber-encased electrical resistance heater with 12 W rating at 24 V was placed just downstream of the plate electrode as a heating source resembling an integrated circuit (IC) chip. Four thermocouples were placed on the corners of a 3 × 3 cm^2 inner square beginning from 2 cm downstream of the plate electrode. The temperature data collected from all four thermocouples were spatially averaged and plotted as a function of time. In the vortex generation case, two needles at span-wise distance of 3 cm were placed at the same height $h = 2.5$ mm with gap $g = 15$ mm. In order to control the direction of the vortex, the applied DC signals of these two needles were kept slightly different (described later).

Fig. 2 shows the PIV data for the velocity field induced by a channel actuator powered with a positive 12 kV DC signal. This was the highest positive voltage that could be applied to the channel while maintaining the steady glow and generating a maximum velocity of 2.6 m/s. PIV results shown on the XZ-plane (Fig. 2(a)) and the XY-plane (Fig. 2(b)) demonstrate the 3-D flow structure generated by a single needle actuated channel flow. Fig. 2(a) shows jet flow covering the entire channel exit in Z-direction with distinct entrainment effects from both sides of the channel. The induced majority airflow covers about 2 cm wide region at the channel exit in the Y-direction. Note that a single needle was powered to create this velocity field. A uniform flow field can be generated by using an array of carefully positioned needles. Also,

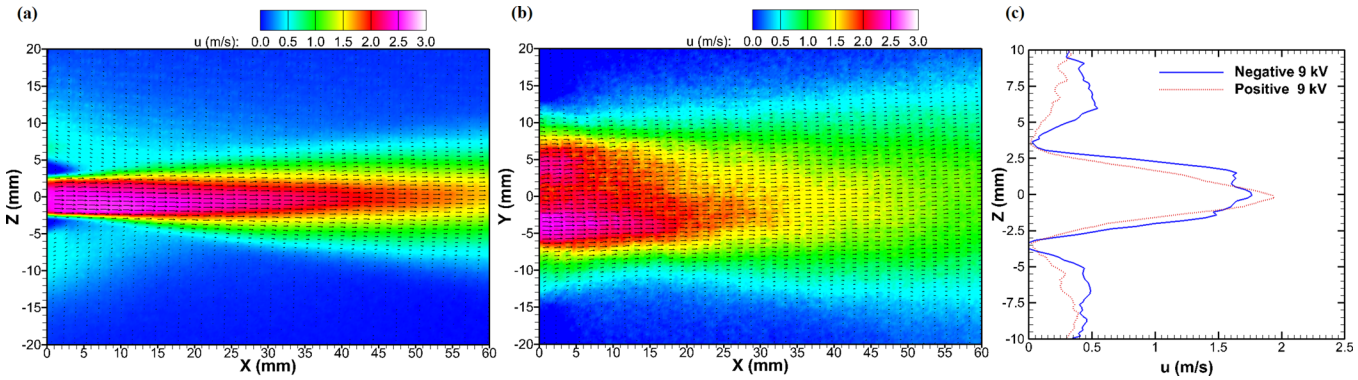

FIG. 2. PIV velocity field for channel actuator operated at positive 12 kV DC signal: (a) XZ-plane and (b) XY-plane. (c) Representative velocity profile comparison for positive and negative 9 kV DC signal at downstream of the exit of the channel actuator at X = 2 mm: along Z-axis.

airflow penetration effect into quiescent surroundings can be noticed in both XY- and XZ-planes.

Fig. 2(c) displays the velocity line profile downstream of the channel exit (X = 2 mm) under different operating signals. In comparison to the positive signal, the velocity profile generated by the negative DC signal is adhering more to the plate electrodes and has a nearly flat middle region. This indicates that the momentum transfer from negative ions to neutral particles mainly happens near the wall. This is evidence for electron attachment occurring outside the ionization zone and around the needle tip. Contrarily, the velocity profile of the positive signal shows a sharp peak at the middle of the channel as displayed in Fig. 2(c), which suggests that the momentum transfer between positive ions and neutral particles mainly happens near the ionization zone around the needle tip. In addition, this phenomenon also suggests that applying a positive signal on the channel configuration will have less wall shear than applying a negative signal. For the span-wise (Y-axis) velocity distribution, both positive and negative signals generate a similar effective region width at 9 kV as the wall effects are minimal for this direction. In addition, induced mechanical power was calculated by integrating measured velocity profiles along the Y- and Z-axes.

Fig. 3 shows the electric power consumptions and maximum velocities as a function of applied voltage for both positive and negative signals in log scale. Interestingly, both power profiles can be characterized by $P \propto V^{\alpha}$ using linear regression with coefficient of determination, $R^2 > 0.99$. The factor α is higher than previously reported result,[2] which is usually 2 to 3. This might be caused by the different electrodes configuration. In channel configuration, not only the corona discharge density but also the corona size and the ion drift zone may increase as the input voltage magnitude increases. More investigation is needed to explain this effect. The power consumption of the negative DC signal ($\alpha = 9.4$) increases even faster than that of the positive DC signal ($\alpha = 5.6$). This difference might be due to the different mechanism of generating working ions. For a positive signal, the majority of positive ions are generated inside the ionization zone near the needle tip. Contrarily, for a negative signal, the majority of negative ions are generated by electron attachment outside the ionization zone. When absolute signal amplitude increases, positive ion generation becomes limited by the size of the ionization zone, while many more electrons can be used to generate negative ions outside the ionization zone. This manifests as a faster growth in peak velocity with voltage for the negative DC input signal. Note that the power consumed by the channel actuator is only several mW, which is extremely low compared to other plasma actuated flows.

Calculated electro-mechanical energy conversion efficiencies for both positive and negative signals are displayed in Fig. 3. Note that the maximum efficiencies for the channel actuator were 2.8% and 1.5% for positive and negative DC signals, respectively. These efficiencies are one order of magnitude larger than the reported efficiency of the surface corona actuators[2] and are about three times the reported efficiency of volume corona actuators.[3] Interestingly, both these values were attained at a magnitude of 7.5 kV DC input. For both positive and negative input voltages, the efficiency increases rapidly from 6 kV to 7.5 kV and then gradually decreases from 7.5 kV to 12 kV. This shows that more energy is wasted at higher voltages. One can also notice that the efficiency of the positive signal is about twice that of the negative signal for the same voltage magnitude. This might be explained by the loss in mechanical power output from wall shear due to the different flow structures mentioned above.

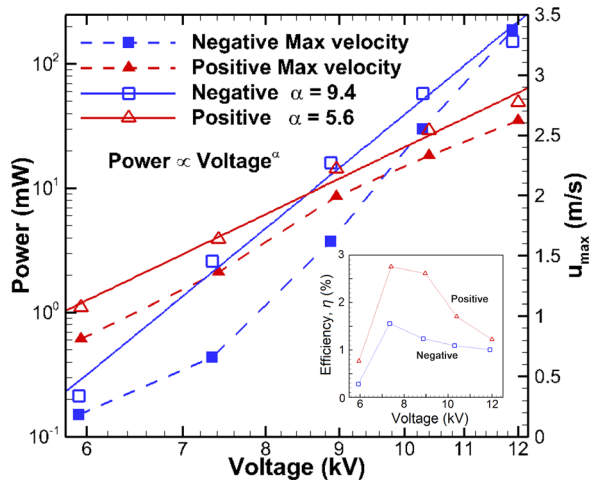

FIG. 3. Performance characterization of the channel actuator: Electrical power consumption and velocity inducement, and (inlay) efficiency of the needle channel.

However, unlike other plasma based flow inducement, the needle actuators can induce a sufficient amount of flow with minute heat generation. This makes it perfectly suitable as a convective cooling device. We demonstrate this cooling capability using a plate-needle configuration with three needles. The arrangement is shown in Fig. 1(c). The surrounding air temperature was $T_\infty = 21\,^\circ\text{C}$. The rubber heater was powered by a 8 V DC signal with an applied surface heat flux of $q'' = 533\,\text{W/m}^2$. Initially, the average temperature of the work surface under free convection was measured at $T_s = 62\,^\circ\text{C}$. Assuming air as an ideal gas, the Grashof number is $Gr = 7.1 \times 10^5$. The convection heat transfer coefficient for this condition may be calculated as $h = 13\,\text{W}/(\text{m}^2 \cdot \text{K})$ by using $q'' = h(T_s - T_\infty)$. Then, the plasma was turned on to measure its cooling effect as a function of positive input voltages and the results were plotted as time varying temperature curves shown in Fig. 4. The convection coefficients with needle actuator were calculated as 15.2, 18.1, and $20.5\,\text{W}/(\text{m}^2 \cdot \text{K})$ with the applied voltages of 6, 9, and 12 kV, respectively. These denote 16.9%, 39.2%, and 57.7% improvement of convective heat transfer, respectively. Specifically, at positive 12 kV, the needle actuator can cool a $3 \times 3\,\text{cm}^2$ area from 62 °C to 47 °C within 80 s. We note that the total power expended by the three needles remains at mW level for each applied voltage (shown in Fig. 4).

Needle actuators may also be used to induce flow vortices near the surface. Two cases were studied by applying slightly different signals on two span wise displaced needle electrodes. We managed to generate a counter-rotating vortex pair between the two needles for which the strength and direction of the majority vortex can be controlled. As displayed in the inlay in Fig. 5(a), needle 1 powered with 10 kV DC signal and needle 2 powered with 8 kV DC signal were separated by a distance $d = 30$ mm. After powering both needles, a counter-clockwise vortex with maximum X-vorticity greater than $300\,\text{s}^{-1}$ was captured using PIV system at YZ-plane with X = 10 mm. Note that the airflow generated by needle 1 is stronger near the wall so that it pushes the airflow generated by needle 2 and then forms a

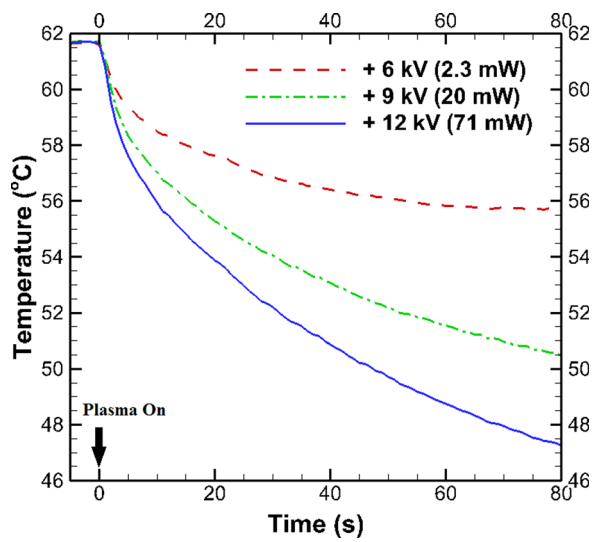

FIG. 4. Transient cooling effect of needle actuator setup (Fig. 1(c)) as function of voltage.

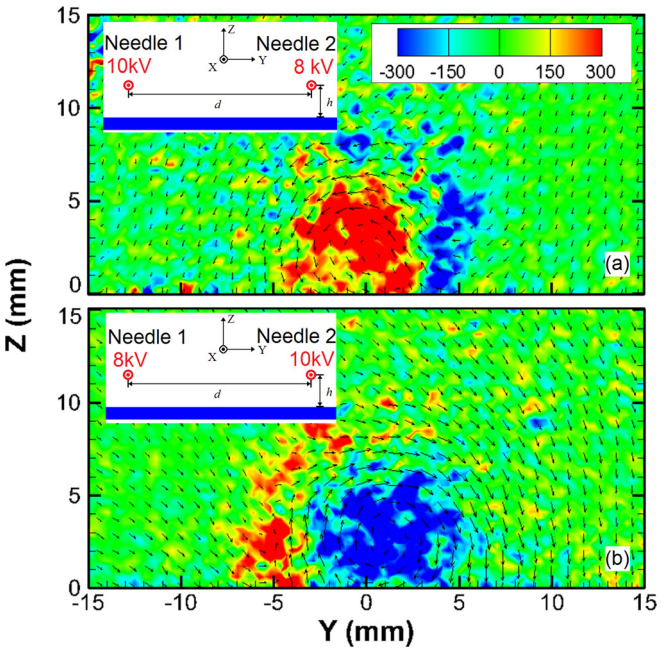

FIG. 5. PIV based demonstration of vortex generation from needle actuator at X = 10 mm downstream (a) majority counter-clockwise and (b) majority clockwise.

counter-clockwise vortex near the wall. For case 2 shown in Fig. 5(b), the needle 2 at Y = 15 mm was powered with a 10 kV DC signal which is higher than the 8 kV DC signal applied to needle 1 at Y = −15 mm. Stronger airflow near the surface was generated near the needle 2 with the majority vorticity generated as clockwise under this condition. Furthermore, the total power used to generate this vortex pair was only 12 mW. To compare this, we assume an incompressible flow over a smooth flat plate at a flight relevant Reynolds number of 1.5×10^7 and estimate the dissipated viscous power using Karman-Schoenherr equation[13] as 548 mW/cm^2 which is at least an order of magnitude larger than the power consumed by the actuator. Therefore, needle actuated vortical flow perturbation may be quite cost-effective for drag reduction, flow mixing, and many other flow control applications.[14]

In summary, the performance and potential applications of the efficient DC needle actuators with channel or plate configuration have been demonstrated. For the channel configuration, momentum was directly injected by a needle-to-plate electrode configuration into the bulk airflow of the channel minimizing the viscous penalty from wall shear stress. Both positive and negative high voltage DC signals were used to generate strong ionic flow in the same direction. However, positive ionic flow with a stronger peak near the center causes less viscous penalty than negative ionic flow adhering to the plate electrodes resulting in higher energy conversion efficiency for positive signal. Combining these characters, the electro-mechanical energy conversion efficiency of such devices can reach 2.8%, almost equal to 4 times that of wire DBD channels[11] or 3 times that of wire corona channels.[3] Some entrainment effect was also observed during the study. The cooling effect and vortex generation using multi-needle plate configuration were also investigated. The study on cooling effects shows that needle actuator can reduce the temperature of a hot area by 15 °C using only mW energy within 80 s.

Controllable vortices generated between 2 needles with different voltages were also demonstrated in the study. Based on these studies, these needle actuator configurations show reasonable potential for many practical applications.

[1]L. Y. Yeo, D. Hou, S. Maheshswari, and H. C. Chang, Appl. Phys. Lett. **88**(23), 233512 (2006).
[2]E. Moreau, J. Phys. D: Appl. Phys. **40**(3), 605–636 (2007).
[3]D. Colas, A. Ferret, D. Pai, D. Lacoste, and C. Laux, J. Appl. Phys. **108**(10), 103306 (2010).
[4]N. Benard and E. Moreau, Appl. Phys. Lett. **100**(19), 193503 (2012).
[5]A. Drews, L. Cademartiri, G. Whitesides, and K. Bishop, J. Appl. Phys. **114**(14), 143302 (2013).
[6]M. Riherd and S. Roy, J. Appl. Phys. **114**(8), 083303 (2013).
[7]T. Jukes, Ph.D. thesis, University of Nottingham, 2007.
[8]D. Go, R. Maturana, T. Fisher, and S. Garimella, Int. J. Heat Mass Transfer **51**, 6047–6053 (2008).
[9]M. Riherd and S. Roy, J. Appl. Phys. **112**, 053303 (2012).
[10]R. Tirumala, N. Benard, E. Moreau, M. Fenot, G. Lalizel, and E. Dorignac, J. Phys. D: Appl. Phys. **47**(25), 255203 (2014).
[11]N. Campbell and S. Roy, Appl. Phys. Lett. **105**(13), 132906 (2014).
[12]R. Durscher and S. Roy, Exp. Fluids **53**(4), 1165–1176 (2012).
[13]H. Schlichting, *Boundary Layer Theory* (McGraw-Hill, 1979).
[14]S. Roy and C. Wang, J. Phys. D: Appl. Phys. **42**, 032004 (2009).